THE JOURNAL OF BIOLOGICAL CHEMISTRY VOL. 283, NO. 45, pp. 30658–30667, November 7, 2008

Paradoxical Effect of Mitochondrial Respiratory Chain Impairment on Insulin Signaling and Glucose Transport in Adipose Cells*

Received for publication, January 22, 2008, and in revised form, July 7, 2008 Published, JBC Papers in Press, September 8, 2008, DOI 10.1074/jbc.M800510200

Xiarong Shi, Alison Burkart, Sarah M. Nicoloro, Michael P. Czech, Juerg Straubhaar, and Silvia Corvera[1]

From the Program in Molecular Medicine, University of Massachusetts Medical School, Worcester, Massachusetts 01605

Adipocyte function is crucial for the control of whole body energy homeostasis. Pathway analysis of differentiating 3T3-L1 adipocytes reveals that major metabolic pathways induced during differentiation involve mitochondrial function. However, it is not clear why differentiated white adipocytes require enhanced respiratory chain activity relative to pre-adipocytes. To address this question, we used small interference RNA to interfere with the induction of the transcription factor Tfam, which is highly induced between days 2 and 4 of differentiation and is crucial for replication of mitochondrial DNA. Interference with Tfam resulted in cells with decreased respiratory chain capacity, reflected by decreased basal oxygen consumption, and decreased mitochondrial ATP synthesis, but no difference in many other adipocyte functions or expression levels of adipose-specific genes. However, insulin-stimulated GLUT4 translocation to the cell surface and subsequent glucose transport are impaired in Tfam knockdown cells. Paradoxically, insulin-stimulated Akt phosphorylation is significantly enhanced in these cells. These studies reveal independent links between mitochondrial function, insulin signaling, and glucose transport, in which impaired respiratory chain activity enhances insulin signaling to Akt phosphorylation, but impairs GLUT4 translocation. These results indicate that mitochondrial respiratory chain dysfunction in adipocytes can cause impaired insulin responsiveness of GLUT4 translocation by a mechanism downstream of the Akt protein kinase.

A large body of evidence has pointed to a close relationship between ectopic fat accumulation in tissues such as muscle and liver and the development of insulin resistance (1–3). The primary defense against such ectopic lipid accumulation is a well functioning adipose tissue, capable of sequestering excess calories in the form of stored triglycerides (4). In addition to this crucial role, adipose tissue is an endocrine organ that controls whole body energy homeostasis by secreting multiple cytokines that signal to other tissues (5, 6). The central role of adipose tissue in energy homeostasis is underscored by recent findings indicating that adipose tissue is a primary locus for the alterations induced by caloric restriction that accompany longevity (7, 8). Thus, the cell biological mechanism involved in optimal adipose tissue development and function are crucial for the control of whole organism energy homeostasis and the determination of life span.

Adipocyte differentiation is accompanied by an expansion of mitochondrial mass (9, 10), but the functional role of the relatively high levels of mitochondria in white adipocytes compared with those in adipose stroma and other tissues is not clear. High mitochondria levels may be required for the support of adipocyte-specific ATP-requiring processes (11), or to support metabolic functions such as glyceroneogenesis, which is required for triglyceride deposition (12, 13). White adipocyte mitochondria levels in rodents and humans change markedly under different physiological conditions, including obesity, weight loss, aging, treatment with anti-diabetic agents, and in response to genetic alterations in insulin receptor number (9, 10, 14–23). Mitochondrial levels correlate with insulin sensitivity, where decreased mitochondrial content correlates with diminished insulin responsiveness, and enhanced mitochondrial mass associates with increased insulin sensitivity. However, given the complexity of whole animal models, a cause-effect relationship between mitochondrial mass and insulin sensitivity in adipocytes has not been established.

Mitochondrial biogenesis depends on a coordinated interaction between nuclear and mitochondrial genomes (24–26). The vast majority of mitochondrial proteins are produced from ~1500 different nuclear localized genes. In contrast, the mitochondrial genome produces only 13 proteins, but among these are key components of the respiratory chain. The replication and transcription of the mitochondrial genome is absolutely dependent on Tfam, a transcription factor encoded in nuclear DNA (27, 28). Tfam is critical for mitochondrial biogenesis during development and for the maintenance of mitochondrial DNA copy number in mature tissues.

To directly determine the functional role of mitochondrial biogenesis in differentiated adipocytes, we have used siRNA[2] to silence of Tfam during the differentiation process. This manip-

* This work was supported, in whole or in part, by National Institutes of Health Grant DK60837. Informatics core services were supported by University of Massachusetts Diabetes and Endocrinology Research Center Grant DK32520. The costs of publication of this article were defrayed in part by the payment of page charges. This article must therefore be hereby marked "*advertisement*" in accordance with 18 U.S.C. Section 1734 solely to indicate this fact.

[1] To whom correspondence should be addressed: Program in Molecular Medicine, University of Massachusetts Medical School, 373 Plantation St., Worcester, MA 01605. Tel.: 508-856-6898; Fax: 508-856-1617; E-mail: silvia.corvera@umassmed.edu.

[2] The abbreviations used are: siRNA, small interference RNA; qRT, quantitative reverse transcription; BSA, bovine serum albumin; PBS, phosphate-buffered saline; mtDNA, mitochondrial DNA; ROS, reactive oxygen species; ERK, extracellular signal-regulated kinase; TIRF, total internal reflection fluorescence; FCCP, carbonyl cyanide-4-(trifluoromethoxy)-phenylhydrazone.

ulation results in the generation of adipocytes that contain only double the mitochondrial levels of pre-adipocytes. Analysis of these cells reveals a specific impairment in insulin-stimulated glucose transport, which occurs distal to early insulin signal transduction events. These results point to a previously unknown interaction between the mitochondrial respiratory chain and insulin sensitivity of the glucose transport pathway and provides evidence that mitochondrial dysfunction could be a primary cause of insulin resistance in adipose cells.

EXPERIMENTAL PROCEDURES

Materials—Real-time PCR primers were designed using the Primer Bank (pga.mgh.harvard.edu/primerbank/index.html). All the PCR primers were synthesized by Operon. Primer sequences are available upon request. Rabbit anti-Tfam antibody was purchased from Aviva Systems Biology; goat anti-Glut4 antibody was from Santa Cruz Biotechnology (Santa Cruz, CA); rabbit anti-Acrp30/adiponectin antibody was from Affinity Bioreagents, Inc.; mouse anti-phospho-Akt and anti-Akt antibodies, and rabbit PAS antibodies (cat # 9611 and #9614, mixed 1:1 and used as a 1:1000 dilution) were from Cell Signaling; mouse anti-phosphotyrosine antibody was from Upstate; and mouse anti-β-Actin antibody was from Sigma.

Cells—3T3-L1 preadipocytes were maintained in Dulbecco's modified Eagle's medium supplemented with 10% fetal bovine serum, 100 units/ml penicillin, and 100 μg/ml streptomycin in an atmosphere of 10% CO_2 at 37 °C (complete medium). Three days post-confluence (day 0), cells were induced to differentiate by adding a hormone mixture (0.5 mM 3-isobutyl-1-methylxanthine, 1 μM dexamethasone, and 5 μg/ml insulin). 72 h later, the differentiation medium was replaced by complete medium, which was replaced every 48 h until analysis.

Transfection—siRNA against mouse Tfam mRNA was purchased from Dharmacon in a duplex form with 3′-dTdT protective overhangs (sense sequence is 5′-GAAUGUGGAUCGUGCUAAAdTdT-3′). At day 2 of differentiation, medium was collected and cells were trypsinized and transfected with Tfam or scrambled siRNA by electroporation. Briefly, 5 nmol of siRNA was used for each 150-mm plate of cells in a 0.4-cm GenePulser® cuvette. After electroporation (180 V, 950 microfarads), cells were resuspended in the collected day 2 medium and re-plated to 6-, 12-, or 24-well plates according to the experiment. 24 h later, the differentiation medium was replaced by complete medium and the medium was refreshed every 2 days afterward.

qRT-PCR—Total RNA were extracted with TRIzol® Reagent. After RNase-free DNase I digestion, RNA was purified with a Qiagen RNeasy® MinElute™ cleanup kit. The purified RNA was then used to synthesize cDNA (iScript™ cDNA Synthesis Kit). Real-time PCR was performed with iQ™ SYBR® Green Supermix on MyiQ single-color real-time PCR detection system from Bio-Rad. The $2^{-\Delta\Delta C_T}$ method was used to analyze the relative mRNA level. Ferritin heavy chain mRNA was used as the internal control.

Western Blotting—Cells were lysed in a buffer composed of 300 mM NaCl, 20 mM NaF, 1 mM $NaPP_i$, 10 mM HEPES, pH 7.4, 1% SDS, and protease inhibitors. 20 μg of cell lysate was resolved on 10% or 15% SDS-PAGE and transferred to nitrocellulose membrane. The blots were blocked with 5% fat-free milk in TBST and incubated with primary antibodies at 4 °C over night. After three washes with TBST and incubation with secondary antibody, the blot was detected by enhanced chemiluminescence (PerkinElmer Life Sciences) and exposure to film.

2-Deoxyglucose Uptake and 3-O-Methylglucose Uptake—Glucose transport was determined by measuring 2-deoxyglucose uptake in a 24-well plate. After 2-h serum starvation in Krebs-Ringer HEPES (KRH) buffer (130 mM NaCl, 5 mM KCl, 1.3 mM $CaCl_2$, 1.3 mM $MgSO_4$, and 25 mM HEPES, pH 7.4, supplemented with 0.5% BSA, and 2 mM sodium pyruvate), the adipocytes were stimulated by insulin for 30 min. Glucose uptake was initiated by addition of [1,2-^{3}H]2-deoxy-D-glucose to a final assay concentration of 100 μM for 5 min at 37 °C. After three washes with ice-cold phosphate-buffered saline (PBS), the cells were lysed with 0.4 ml of 1% Triton X-100. The ^{3}H was then determined by scintillation counting. Nonspecific 2-deoxyglucose uptake was measured in the presence of 20 μM cytochalasin B and subtracted from each determination. 3-*O*-Methylglucose uptake was carried out in a similar way with the following differences: instead of 2-deoxyglucose, the 3-*O*-[*methyl*-^{14}C]-D-glucose was added to the cells to 35.4 μM and allowed to be incubated for 60 s. Cells were then washed three times with cold PBS plus 1 mM $HgCl_2$.

Flow Cytometry—Cells were trypsinized and incubated in KRH buffer without or with 100 nM MitoTracker® Green^{FM} for 30 min at 37 °C. 1×10^6 cells were then resuspended in 1 ml of ice-cold phosphate-buffered saline with 0.5% BSA and analyzed on an LSR II cytometer analyzer (BD Biosciences). Data were gated using non-stained cells to represent MitoTracker® Green^{FM} staining.

Mitochondrial DNA Measurement—Total DNA was extracted by DNeasy® tissue kit. Primer pairs corresponding to Nd1 (mitochondrial) and Actb (nuclear) were used to amplify a mitochondrial and nuclear DNA fragment, respectively. The $2^{-\Delta\Delta C_T}$ method was used to analyze the relative mtDNA level.

Oxygen Consumption Assay—The oxygen consumption was measured using live intact cells with BD™ Oxygen Biosensor System. Cells (500,000 cells/ml) were suspended in KRH buffer supplemented with 0.5% BSA and 2 mM pyruvate. 150 μl of cell suspension was added to triplicate wells in an Oxygen Biosensor System 96-well plate. Fluorescence signal was read using a TECAN Safire^2 microplate reader continuously every 2 min at 37 °C. Oxygen concentration was calculated from the fluorescence intensity according to the manufacturer's instructions.

ATP Measurement—ATP level was measured using a CellTiter-Glo® Luminescent Cell Viability Assay (Promega, Madison, WI). Equal numbers of control or knockdown cells were trypsinized and incubated in an opaque 96-well plate in six replicates for 1 h. 100 μl of the reaction reagent was directly added to each well, and after 10 min the luminescence signal was detected using a microplate reader. To measure ATP synthesis dynamically, cells were first suspended in respiration buffer (0.1% BSA, 75 mM mannitol, 25 mM sucrose 100 mM KCl, 10 mM KH_2PO4, 5 mM $MgCl_2$, 20 mM, Tris, pH 7.5, 10^6 cells/ml), and 10 μg/ml digitonin was added for 5 min. Digitonin was removed by resuspending the permeabilized cell in the same volume of respiration buffer. Vehicle or 10 μg/ml oligomycin

TABLE 1
Number of probes displaying changes at specific intervals during differentiation

Probe signal > 50 on any day						
Interval	Probes increased > 1.25	Probes decreased > 1.25	Probes unchanged	Mito Probes increased > 1.25	Mito Probes decreased > 1.25	Mito Probes unchanged
Days 0–6	2,834	3,374	32,265	530	70	985
Days 0–2	19	20	38,967	0	2	1,711
Days 2–4	2,229	1,888	35,148	435	37	1,126
Days 4–6	342	496	36,976	37	13	1,529
Probe signal > 1500 on any day						
Interval	Probes increased > 1.5	Probes decreased > 1.5	Probes unchanged	Mito Probes increased > 1.5	Mito Probes decreased > 1.5	Mito Probes unchanged
Days 0–6	807	677	2,541	294	15	254
Days 0–2	1	0	3,549	0	0	412
Days 2–4	631	327	3,202	233	11	322
Days 4–6	35	34	3,552	7	1	564

was added and mixed well by gentle inverting. 100 μl of cell suspension were then transferred to wells of a 96-well plate, which contained substrates (1 mM ADP and 10 mM succinate final concentration) for different time periods. ATP synthesis was stopped by adding 100 μl of CellTiter-Glo® reagent and luminescence was read using a Safire^2 microplate reader. ATP synthesized from mitochondria was derived by subtracting the oligomycin-treated reading from those untreated.

Reactive Oxygen Species Measurement—Cells were seeded to a 24-well plate in medium without phenol red, and incubated without or with 50 ng/ml TNFα for 3 h. Following two washes with PBS, cells were incubated with 10 μM 5-(and 6-)chloromethyl-2′,7′-dichlorodihydrofluoresceindiacetate, acetyl ester (CM-H_2DCFDA) (Invitrogen) in Krebs-Ringer bicarbonate buffer for 15 min at 37 °C. The fluorescent signal was read at excitation of 485 nm and emission of 530 nm in a microplate reader.

Triglyceride Content Measurement—Cells in 6-well multiwell dishes were scrapped into 200 μl of PBS and sonicated for 20 s on ice. The lysate was subject to total glycerol determination using a Serum Triglyceride Determination Kit (Sigma, TR0100). Briefly, 10 μl of lysate or standard was mixed with 1 ml of Triglyceride Working Reagent and incubated for 30 min at 37 °C. The absorbance was read at 540 nM, and glycerol concentration was then calculated from the standard curve.

Oil Red O Staining—Cells were washed with PBS twice and fixed in 4% formaldehyde for 1 h at room temperature. After three washes with water, the cells were incubated with 5 mg/ml Oil Red O in 60% triethyl phosphate for 30 min. Cells were then washed with water at least six times before imaging.

Total Internal Reflection Fluorescence Microscopy—Cells seeded on coverslips were serum-starved for 2 h in KRH buffer supplemented with 0.5% BSA and 2 mM pyruvate and were then stimulated by 0, 0.1, or 1 μM insulin for 30 min. Cells were fixed in 4% paraformaldehyde for 15 min at room temperature, permeabilized with 0.5% Triton X-100 plus 1% fetal bovine serum in PBS, and stained with goat anti-Glut4 (1:200) antibodies overnight at 4 °C. Alexa Fluor® 488 donkey anti-goat secondary antibodies were used to detect bound primary antibody. TIRF images were taken for 10 random fields from each coverslip. Background areas containing no cells were used to threshold the images, and the total fluorescence intensity of the whole area was then obtained.

Affymetrix GeneChip Expression Analysis—Total RNA was prepared from three 150-mm dishes of 3T3-L1 cells at each day of differentiation. Affymetrix protocols were followed for the preparation of cRNA from total RNA, which was hybridized according to Affymetrix instructions to a MOE430-2 Chips. The GeneChips were washed with a GeneChip Fluidics Station 400 and were scanned with an HP GeneArrayScanner (Affymetrix). Raw expression data were analyzed with the Bioconductor statistical environment using RMA and MAS5, a Bioconductor implementation of the MAS 5.0 algorithm (Affymetrix). The "-fold change" for each gene was determined by dividing the mean of the average difference from three independent experiments.

RESULTS

Previously we have found that differentiation of 3T3-L1 adipocytes is accompanied by increased mitochondrial biogenesis, assessed primarily by mass spectrometry of peptides increased during adipogenesis (9). A more in-depth analysis of Affymetrix databases obtained from 3T3-L1 cells at different days during differentiation reveals that a marked increase in expression of mitochondrial genes occurs between days 2 and 4 of differentiation. This is the period at which the most pronounced changes in gene expression occur, evidenced by the many changes in both non-mitochondrial and mitochondrial transcripts (Table 1). Of all transcripts changed between days 2 and 4 of differentiation, approximately half were increased and half decreased (2229 increased, 1888 decreased by >1.25-fold between days 0 and 6 of differentiation). In contrast, of the transcripts identified by the gene ontology term "mitochondrion," many more were increased than decreased in the same interval (435 increased, 37 decreased by >1.25-fold). The overrepresentation of mitochondrial genes in the pool of genes that increased during differentiation was also seen when only high abundance (*i.e.* signals > 1500) genes undergoing changes of >1.5-fold were counted (Table 1, lower half). Their high representation is also reflected when the numerical averages of all observed changes are plotted (Fig. 1*A*). The predominant increase in mitochondrial gene expression occurs between days 2 and 4 of differentiation and is stable thereafter (Fig. 1*A*). The relevance of mitochondrial gene expression during adipocyte differentiation is underscored by pathway analysis using the Kyoto Encyclopedia of Genes and Genomes (29). The top 20 pathways that are highly enriched in genes that increase during adipocyte differentiation are shown in Table 2; 14 of these pathways, including the top 5, are mitochondrial metabolic pathways.

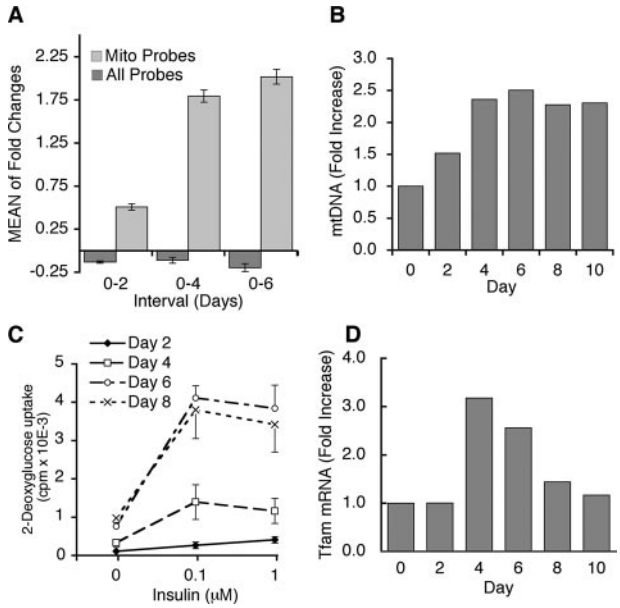

FIGURE 1. **Changes in mitochondrial gene expression during 3T3-L1 adipocyte differentiation.** *A*, "*All probes*" refers to those detected with the MOE430-2 Affymetrix GeneChip, with a signal > 50. "*Mito Probes*" refers to probes annotated with gene ontology cellular component term "mitochondrion" retrieved directly from the Affymetrix website. Plotted are the average of all -fold increases and decreases in probe signal between the days of differentiation indicated on the abscissa. *B*, total DNA was extracted at the days indicated on the abscissa. Mitochondrial DNA (*mtDNA*) copy number was determined by qRT-PCR taking nuclear DNA as internal control and expressed as -fold change over day 0 of differentiation. *C*, the uptake of 2-deoxyglucose was measured after 30 min of incubation with the indicated concentrations of insulin at the times of differentiation indicated. *Points* represent means, and *lines* ±S.E. of two independent experiments performed in triplicate. *D*, Tfam mRNA expression determined by qRT-PCR, using ferritin mRNA as internal control and expressed as -fold change over day 0 of differentiation.

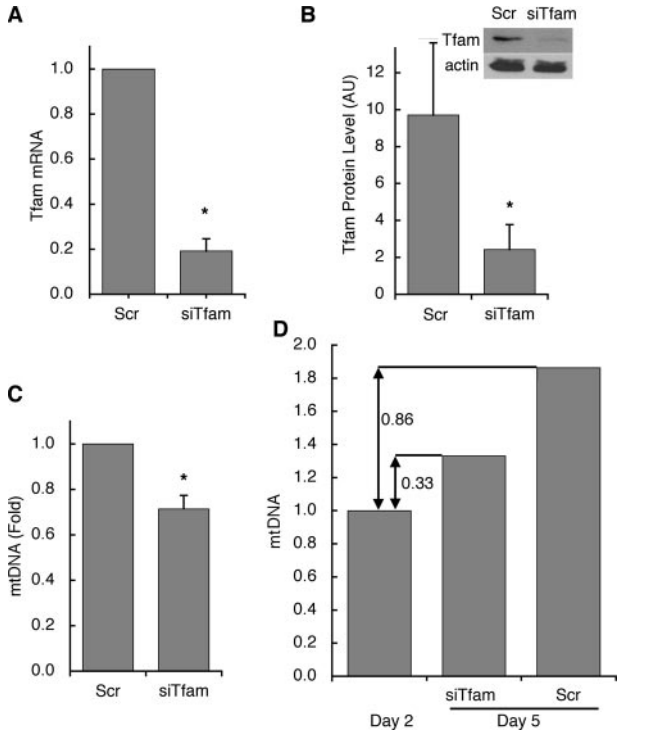

FIGURE 2. **Inhibition of Tfam induction and mtDNA amplification by siRNA against Tfam.** Cells were transfected with scrambled (*Scr*) or Tfam-directed (*siTfam*) siRNA oligonucleotides at day 2 of differentiation. 72 h later: *A*, Tfam mRNA levels were determined by qRT-PCR. *B*, Tfam protein levels were analyzed by Western blotting and densitometry. Actin levels are included as a loading control. *C*, mtDNA copy number was assessed relative to nuclear DNA. *D*, comparison of mtDNA increase from the time of transfection (day 2) to day 5, in cells transfected with scrambled or Tfam-directed siRNA oligonucleotides. *, $p < 0.05$ relative to Scr, using two-tailed paired Student *t* tests with a minimum of three independent experiments.

TABLE 2

Top 20 Kyoto Encyclopedia of Genes and Genomes (KEGG) pathways enriched for genes that increase between days 0 and 6 of differentiation

M	KEGG pathway	*p* value
*[a]	Oxidative phosphorylation	<2.22e−16
*	Valine, leucine, and isoleucine degradation	<2.22e−16
*	Citrate cycle (trichloroacetic acid cycle)	<2.22e−16
*	Glycolysis/gluconeogenesis	<2.22e−16
*	Pyruvate metabolism	<2.22e−16
	Carbon fixation	<2.22e−16
	Pentose phosphate pathway	<2.22e−16
*	Fatty acid metabolism	<2.22e−16
*	Butanoate metabolism	<2.22e−16
*	Fatty acid elongation in mitochondria	<2.22e−16
*	Propanoate metabolism	<2.22e−16
	Glycerophospholipid metabolism	<2.22e−16
*	ATP synthesis	<2.22e−16
*	Lysine degradation	<2.22e−16
*	Benzoate degradation via CoA ligation	<2.22e−16
	Insulin signaling pathway	<2.22e−16
*	Reductive carboxylate cycle (CO_2 fixation)	4.29E−16
*	Glyoxylate and dicarboxylate metabolism	4.80E−16
	Biosynthesis of steroids	9.69E−15
	Starch and sucrose metabolism	2.01E−14

[a] * indicates a mitochondrial metabolic pathway (*M*).

The pronounced changes in expression of mitochondrial proteins could produce mitochondrial remodeling, without necessarily requiring mitochondrial biogenesis, understood here as a process of expansion of mitochondrial mass and mitochondrial DNA copy number. Nevertheless, a significant increase in mitochondrial DNA did occur between days 2 and 4 of differentiation (Fig. 1*B*). Importantly, this increase coincided with the differentiation-dependent induction of insulin responsiveness, as seen by the magnitude of the effect of insulin on the stimulation of glucose transport at different days of differentiation (Fig. 1*C*). Mitochondrial DNA replication requires the transcription factor Tfam, and indeed Tfam mRNA increased significantly between days 2 and 4 of differentiation (Fig. 1*D*). Interestingly, although the levels of mitochondrial DNA remained high after day 4 of differentiation, Tfam levels decreased, suggesting that the maintenance of mitochondrial DNA in these cells is not sensitive to Tfam levels over this short time period. These results also suggest that interference with Tfam induction prior to day 4 of differentiation could produce cells harboring a selective impairment in those mitochondrial functions dependent on mitochondrial DNA-encoded transcripts.

The effectiveness of Tfam knockdown by siRNA oligonucleotides, introduced on day 2 of differentiation, was evaluated by measuring both mRNA and protein levels at day 5 of differentiation. Compared with cells electroporated with scrambled control oligonucleotides, Tfam knockdown cells displayed an 80% reduction in Tfam mRNA (Fig. 2*A*). Tfam protein levels, evaluated by Western blotting, were concomitantly reduced by ~70% (Fig. 2*B*). Tfam knockdown led to a 30% decrease in mtDNA copy number compared with cells electroporated with scrambled control oligonucleotides (Fig. 2*C*). Thus, whereas in

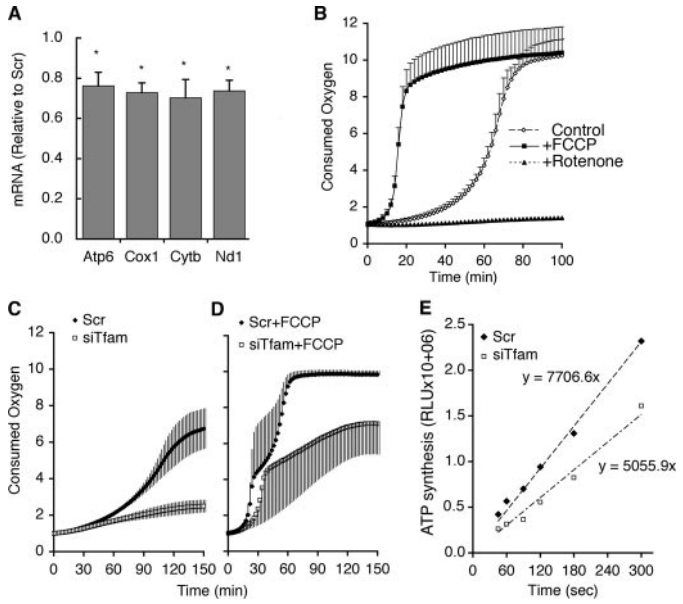

FIGURE 3. **Decreased levels of mitochondrial DNA-encoded genes and respiratory chain function in Tfam knockdown cells.** *A*, mRNA levels of four mtDNA encoded genes determined at day 5 in cells transfected at day 2 with scrambled (*Scr*) or Tfam-directed (*siTfam*) siRNA oligonucleotides. *Bars* represent values in siTfam cells relative to Scr. Statistical significance was calculated using two-tailed paired Student *t* tests; *, $p < 0.05$. *B*, adipocytes at day 6 were aliquoted into a BD Oxygen Biosensor System 96-well plate. FCCP or rotenone was added, and recording of fluorescence was immediately initiated. *C* and *D*, control and Tfam knockdown cells at day 5 were aliquoted into a BD Oxygen Biosensor System 96-well plate and fluorescence was recorded in the absence (*C*) or presence (*D*) of FCCP. Fluorescence was monitored every 2 min at 37 °C and is expressed as fluorescence units relative to time 0 values. Plotted are the means, and *vertical lines* represent ±S.E. of three independent experiments preformed in triplicate. *p* values obtained from paired two-tailed Student *t* tests of the means were: 3.1E−17 for Scr *versus* siTfam; 5.2E−32 for Scr *versus* Scr+FCCP; 9.9E−34 for Scr+FCCP *versus* siTfam+FCCP; and 1.7E−35 for siTfam *versus* siTfam+FCCP. *E*, mitochondrial ATP production in digitonin-permeabilized cells. Shown is a representative example of three independent experiments performed in triplicate. *p* value obtained from paired two-tailed Student *t* tests from the means of three experiments was 0.0025 for Scr *versus* siTfam.

control cells mtDNA increased by ~2-fold from days 2 to 5, in the Tfam knockdown cell mtDNA increased by only ~33% (Fig. 2*D*). Consistent with our observation that Tfam does not appear to be absolutely required for maintenance of mtDNA in these cells over the period of time studied, mtDNA was not reduced when Tfam siRNA was introduced at day 6 of differentiation and mtDNA copy number measured at day 9 (data not shown).

Because transcripts from mtDNA might be expected to have different lifetimes than mtDNA itself, we tested the effect of siRNA against Tfam on genes encoded by mtDNA. Nd1, Cytb, Cox1, and Atp6 encode for polypeptides that form part of respiratory chain complexes I, III, IV, and V, respectively. The levels of all four of these transcripts were reduced by ~30% in cells transfected with siRNA against Tfam compared with scrambled control (Fig. 3*A*). We then investigated if the reduced mtDNA expression of these subunits had a functional effect on electron transport. Oxygen is consumed in the end step of the respiratory chain. Thus, the rate of oxygen consumption provides a global estimate of the functionality of the entire respiratory chain. Oxygen consumption can be measured in 96-well multiwell plates using the BD™ Oxygen Biosensor System, in which the quenching by ambient oxygen of a fluorophore embedded on the bottom of the well is measured continuously in a fluorescence microplate reader. Fig. 3*B* illustrates the typical readout from this assay, where quenching occurs in a non-linear fashion, which depends on the number of cells plated, and is responsive to changes in respiratory rate, as seen in the accelerated response in cells pre-treated with carbonyl cyanide-4-(trifluoromethoxy)-phenylhydrazone (FCCP), and the impaired response in cells pretreated with rotenone, an inhibitor of complex I. The activity of the electron transport chain was significantly impaired as estimated by the decrease in oxygen consumption seen in Tfam knockdown cells compared with controls (Fig. 3*C*). This impairment persisted in the presence of FCCP, which by uncoupling the proton gradient maximizes electron transport and thereby oxygen consumption. Thus, the maximal capacity of the electron transport chain was diminished in adipocytes in which Tfam induction was impaired during differentiation.

As an alternative way to monitor the activity of the electron transport chain, the capacity of mitochondria to synthesize ATP was measured. Digitonin-permeabilized adipocytes were incubated in the presence or absence of oligomycin-A, to inhibit the activity of the mitochondrial ATPase. ATP synthesis driven by ADP and succinate was then measured dynamically using a luciferase-based ATP assay. Mitochondrial ATP synthesis was obtained by subtracting the values obtained in the presence from those in the absence of oligomycin-A. A significant impairment in mitochondrial ATP production was seen in Tfam knockdown cells compared with controls (Fig. 3*E*), whereas no difference was seen in non-mitochondrial ATP levels, which remained unchanged during the incubation (not illustrated).

The vast majority of mitochondrial proteins is encoded by nuclear DNA. To determine whether siRNA to Tfam might indirectly affect the expression of nuclear-encoded mitochondrial genes, we examined the levels of mRNA for enzymes involved in the tricarboxylic acid cycle, fatty acid oxidation, and oxidative phosphorylation. No significant changes in these mRNAs were seen in response to Tfam knockdown (Fig. 4*A*). Moreover, functional assessment of fatty acid oxidation using exogenous palmitate revealed no significant changes in response to Tfam knockdown (not illustrated). We also determined the expression of a group of nuclear encoded regulators of mitochondrial biogenesis, which were also unchanged in Tfam knockdown cells (Fig. 4*B*). Consistent with a lack of effect of Tfam depletion on non-mtDNA encoded mitochondrial genes, the overall cellular abundance of mitochondria assessed by staining with specific fluorescence marker MitoTracker® Green^{FM} was found to be unchanged in Tfam knockdown cells; neither fluorescence-activated cell sorting analysis of live cells stained with MitoTracker® Green^{FM} (Fig. 4*C*) nor visual inspection of individual cells (Fig. 4*D*) revealed any detectable difference in density or mitochondrial morphology.

Alterations in adipose tissue mitochondrial gene expression correlated with insulin sensitivity in animal models, but this correlation may be spurious, or perhaps even secondary to altered insulin sensitivity. 3T3-L1 adipocytes depleted of Tfam provide a straightforward model system to determine whether

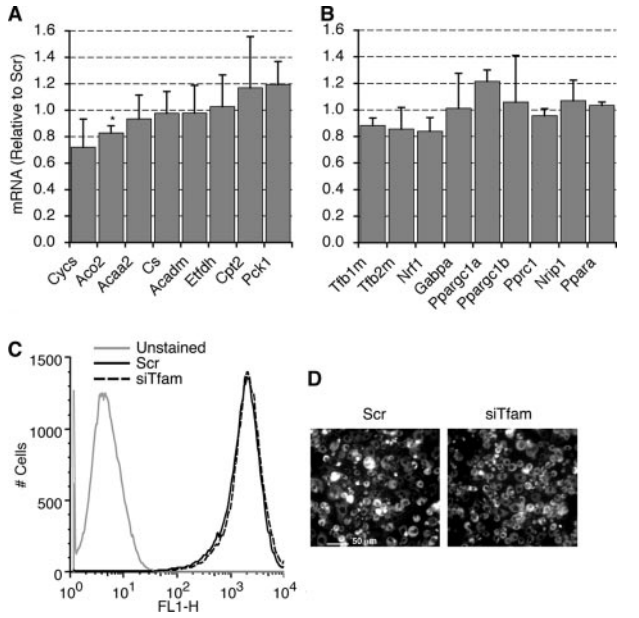

FIGURE 4. **Nuclear encoded mitochondrial gene expression and mitochondrial mass in Tfam knockdown cells.** The relative mRNA level of various nuclear-encoded mitochondrial genes (*A*) and nuclear encoded mitochondrial related regulators (*B*) was determined by qRT-PCR at day 5 in cells transfected at day 2 with scrambled or Tfam-directed siRNA oligonucleotides. Results are expressed relative to scrambled control values. Cells were stained with MitoTracker Green and subjected to fluorescence-activated cell sorting analysis (*C*) or visualized by fluorescence microscopy (*D*).

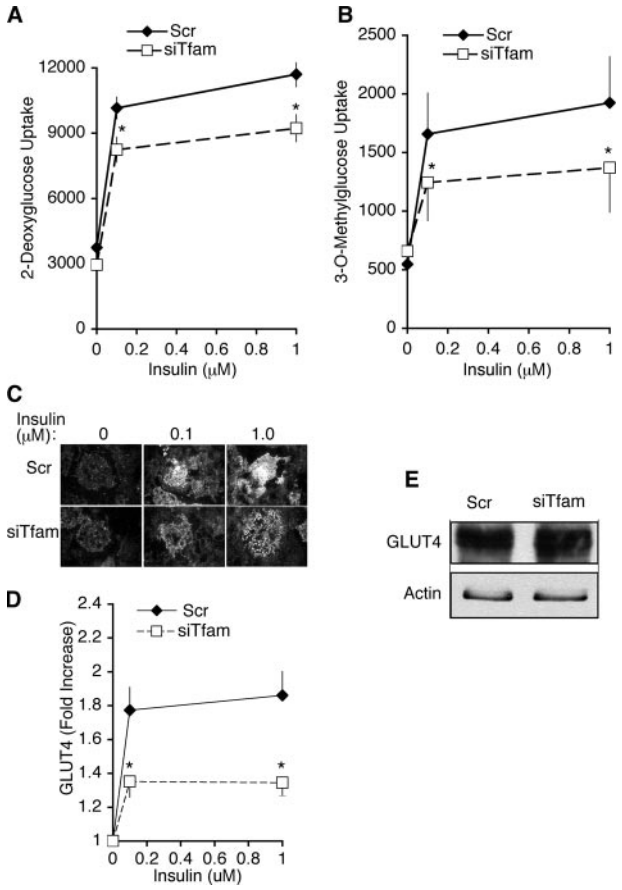

FIGURE 5. **Glucose transport and GLUT4 trafficking in Tfam knockdown cells.** Cells were transfected with scrambled (*Scr*) or Tfam-directed (*siTfam*) siRNA oligonucleotides at day 2 of differentiation. At day 6, cells were serum-starved for 2 h; *A*, the uptake of 2-deoxyglucose was measured after 30 min of incubation with the indicated concentrations of insulin. *Points* represent means, and *lines* are ±S.E. of three independent experiments performed in triplicate. *p* values obtained by two-tailed paired Student *t* tests were 0.0039 and 0.0057 for Scr *versus* siTfam at 0.1 and 1 μM insulin, respectively. *B*, measurement of 3-*O*-methylglucose under the same conditions as in *A*. *p* values obtained by two-tailed paired Student *t* tests were 0.07 and 0.0025 for Scr *versus* siTfam at 0.1 and 1 μM insulin, respectively. Cells treated with the indicated concentrations of insulin were fixed and stained with antibodies to endogenous GLUT4 and imaged by TIRF. *C*, representative images of random fields; *D*, quantification of average intensity of random fields. *Points* represent means of four independent experiments from which 10 random fields from each coverslip were averaged. *Lines* represent ± S.E. *p* values obtained by two-tailed paired Student *t* tests were 0.008 and 0.006 for Scr *versus* siTfam at 0.1 and 1 μM insulin, respectively. *E*, representative Western blot of GLUT4 in cells transfected with scrambled (*Scr*) or Tfam-directed (*siTfam*) siRNA oligonucleotides at day 2 of differentiation and lysed at day 6. Similar results were obtained in three independent experiments.

impairment of adipose respiratory chain function can affect insulin sensitivity. To this end, we examined the effects of insulin on glucose uptake in Tfam-depleted cells. Preadipocytes were transfected with Scr or Tfam-directed siRNA oligonucleotides at day 2 of differentiation, and glucose transport was measured at day 6. A clear response to insulin to stimulate 2-deoxyglucose uptake could be observed at day 6 (Fig. 5*A*). Although Tfam depletion did not significantly affect basal 2-deoxyglucose uptake, the stimulatory effect of insulin was significantly impaired in Tfam knockdown cells (Fig. 5*A*). To rule out the possibility that impaired insulin responsiveness could be due to off-target effects of the silencing oligonucleotides, cells were electroporated on day 6 of differentiation, and glucose uptake was measured on day 8, a period during which Tfam-directed siRNA has no effect on Tfam levels, as described above. No differences in basal or insulin-stimulated glucose uptake were seen between cells transfected with Scr or Tfam-directed siRNA at day 6 (4508 ± 212 *versus* 4433 ± 298 cpm Scr or Tfam-directed siRNA in response to 0.1 μM insulin). Thus, impairment of insulin-stimulated glucose uptake correlates specifically with suppression of Tfam induction.

Impaired 2-deoxyglucose uptake can result from a decreased rate of glucose transport across the plasma membrane, or from a decreased rate of phosphorylation of 2-deoxyglucose by hexokinase. To distinguish between these possibilities, we measured the uptake of 3-*O*-methylglucose in response to insulin, which specifically reflects transport, and found that it was also impaired by Tfam depletion (Fig. 5*B*). Thus impairment in respiratory chain function results in impaired insulin action to stimulate glucose transport, independently of glucose metabolism.

To determine whether decreased insulin-stimulated glucose transport was due to alterations in GLUT4 translocation to the cell surface, we analyzed GLUT4 trafficking using total internal reflection fluorescence (TIRF). This imaging technique allows the specific visualization of fluorophores residing ~100 nm from the plasma membrane (30). Because insulin stimulates translocation of GLUT4 to the TIRF zone as well as fusion with the plasma membrane (31), TIRF imaging of endogenous GLUT4 provides a direct estimation of insulin action on GLUT4 trafficking. Insulin-stimulated recruitment of endogenous GLUT4 to the TIRF zone was significantly impaired in Tfam knockdown cells (Fig. 5, *C* and *D*). This decrease did not result from decreased protein levels of GLUT4, assessed by

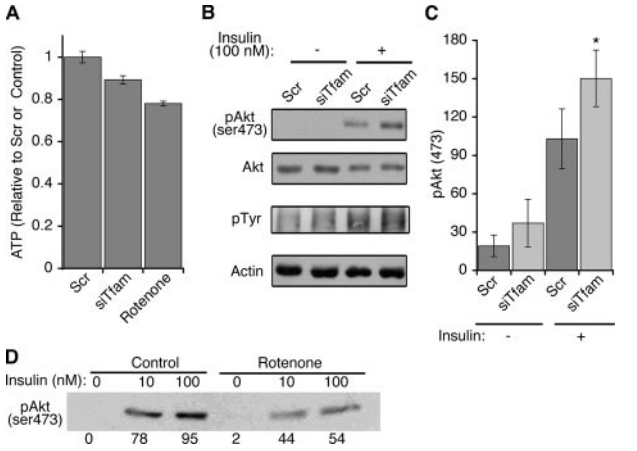

FIGURE 6. **ATP levels and insulin signaling in Tfam knockdown cells.** *A*, cells were transfected with scrambled (*Scr*) or Tfam-directed (*siTfam*) siRNA oligonucleotides at day 2 of differentiation, and at day 6 ATP levels were determined by luminescence. Where indicated, rotenone (5 μM) was added to control cells for 60 min prior to measurement. *Bars* are means, and *lines* are ±S.E. of three experiments performed in triplicate. *p* values obtained by one-tailed paired Student *t* tests were 0.048 and 0.00018 Scr *versus* siTfam and control *versus* rotenone, respectively. *B*, cells prepared as above were stimulated with 10 nM insulin for 15 min and then harvested in lysis buffer with phosphatase and protease inhibitors. Western blots were performed using antibodies to phospho-Akt (serine 473) and phosphotyrosine antibody (4G10), respectively. Shown is the area of the gel (~180 molecular weight) showing maximal stimulation in phosphotyrosine signal. Antibodies to total Akt and actin were used to control for loading. *C*, quantification of Akt phosphorylation from four independent experiments. *, *p* value obtained by one-tailed Student *t* tests was 0.031 for Scr *versus* siTfam in the presence of insulin. *D*, adipocytes at day 6 of differentiation were treated without (*Control*) or with 500 nM rotenone for 60 min, and then with the indicated concentrations of insulin for 15 min prior to lysis and Western blotting with anti-phospho Akt antibody. The values from the densitometry scan of this representative experiment are shown below each band.

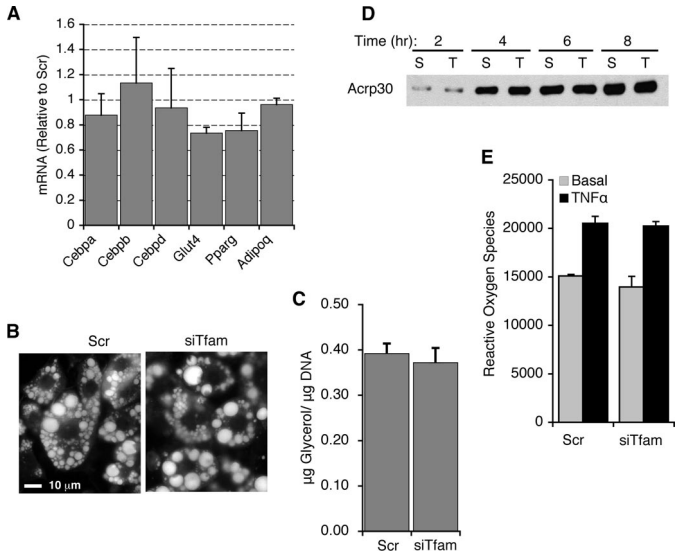

FIGURE 7. **Adipocyte functions in Tfam knockdown cells.** *A*, the relative mRNA level of various transcription factors and adipocyte-specific proteins was determined by qRT-PCR at day 5 in cells transfected at day 2 with scrambled or Tfam-directed siRNA oligonucleotides. Results are expressed relative to scrambled values. *B* and *C*, Oil red O staining and triglyceride content of cells at day 5. *D*, cells were washed in PBS and placed in fresh medium. An aliquot of the medium was collected at the time points indicated and analyzed by Western blotting with an antibody to adiponectin (*Acrp30*). *E*, cells were incubated without or with 50 ng/ml TNFα for 3 h, and reactive oxygen species were measured by 5-(and 6-)chloromethyl-2′,7′-dichlorodihydrofluoresceindiacetate, acetyl ester fluorescence, detected directly in cells grown on 24-well multiwell plates using a TECAN Safire^2 microplate reader.

Western blot analysis of total cell extracts (Fig. 5*E*). Thus, insulin stimulation of GLUT4 translocation and subsequent glucose transport are impaired in adipocytes with decreased respiratory chain function.

One possible mechanism by which insulin-simulated glucose uptake might be impaired in Tfam knockdown cells would be through decreased ATP levels, which would in these cells lead to impairment in insulin signal transduction (11). Steady-state ATP levels in Tfam knockdown cells were indeed decreased, albeit only by a small (~10%) amount (Fig. 6*A*). This decrease did not result in impaired insulin signaling, as assessed by the levels of tyrosine phosphorylation and Akt phosphorylation in response to insulin (Fig. 6*B*). Indeed, a highly reproducible increase in Akt phosphorylation was consistently observed in Tfam knockdown cells (Fig. 6*C*). This effect contrasted markedly with that seen in response to rotenone, an acute inhibitor of Complex 1. After 60 min, rotenone decreased ATP levels by an amount only slightly greater than that produced by Tfam knockdown (Fig. 6*A*). However, rotenone treatment markedly impaired insulin-stimulated Akt phosphorylation (Fig. 6*D*) and adiponectin secretion (data not shown). These results point to important differences in cellular response to acute *versus* progressive impairment of electron transport. A large, transient decrease in ATP levels and stimulation of glucose uptake are known to occur within minutes after rotenone exposure (32). These changes are not observed in Tfam knockdown cells, where Complex I dysfunction is probably less severe than that elicited by direct chemical inhibition, and in which compensatory changes can occur during several days of differentiation.

The observed small decrease in ATP levels and impaired respiratory chain function in Tfam knockdown cells was also without a detectable effect on numerous parameters that reflect basic functional characteristics of differentiated adipocytes, including mRNA levels of adipogenic genes (Fig. 7*A*), triglyceride accumulation (Fig. 7, *B* and *C*), and basal adiponectin secretion (Fig. 7*D*). This later lack of effect is also indicative of the differences between acute *versus* chronic impairment in respiratory chain function, as adiponectin secretion has been shown to decrease in response to acute inhibition of mitochondrial ATP synthesis, and is not inconsistent with prior studies where Tfam depletion mitigates the enhancement of adiponectin secretion seen in response to enhanced mitochondrial biogenesis (33). Thus, the results shown here indicate that progressive impairment of respiratory chain function through Tfam knockdown in adipocytes leads to impaired insulin-stimulated glucose uptake, by a mechanism probably unrelated to changes in ATP levels. Moreover, insulin signaling to Akt is in fact significantly increased in cells with impaired respiratory chain function.

Other signaling pathways in adipocytes that involve mitochondrial function include those elicited by inflammatory cytokines. The effects of TNFα, for example, involve changes in mitochondrial reactive oxygen species (ROS) production (34, 35). To explore whether this pathway would be affected in cells depleted of mtDNA, control and Tfam knockdown adipocytes were treated with 50 ng/ml TNFα, and ROS was then measured in live cells. Basal ROS production was indistinguishable between control and Tfam knockdown cells, as

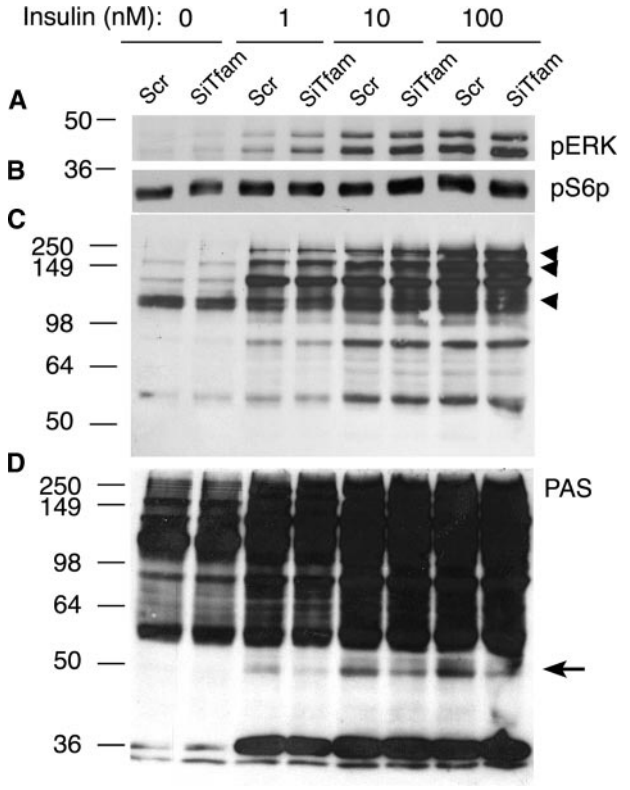

FIGURE 8. **Effect of Tfam knockdown on insulin signaling pathways.** Cells were transfected with scrambled (*Scr*) or Tfam-directed (*siTfam*) siRNA oligonucleotides at day 2 of differentiation, and at day 6 were stimulated with the indicated concentrations of insulin for 15 min prior to harvest in lysis buffer with phosphatase and protease inhibitors. Western blots were performed using antibodies to ERK1 and -2 (*A*), Phospho S6 protein (*B*), and PAS antibodies (*C* and *D*). Shown are representative blots at lower (*C*) or higher (*D*) exposures. *Arrowheads* point to substrates that were increased, and the *arrow* points to one substrate detected that was decreased by Tfam knockdown. Similar results were obtained in three independent experiments.

was the 40% increase in ROS production elicited by TNFα (Fig. 7*E*). Thus, chronic impairment in respiratory chain function results in a specific impairment of glucose transport stimulation by insulin, without detectable effects on multiple other adipocyte-specific functions or signal transduction events.

To better understand the mechanism by which insulin signaling to glucose transport might be affected by Tfam knockdown, additional pathways downstream of insulin receptor activation were analyzed. Neither the stimulation of ERK1 and -2 phosphorylation (Fig. 8*A*), nor the phosphorylation of the S6 protein (Fig. 8*B*) by insulin were significantly affected by Tfam knockdown. To analyze whether the observed enhancement of Akt phosphorylation seen in Tfam knockdown cells was accompanied by changes in the phosphorylation of Akt substrates, we utilized phospho-specific antibodies directed to Akt substrates (*PAS*, Fig. 8, *C* and *D*) (36, 37). Several insulin-stimulated phosphoproteins could be observed, including bands at ~75, 105, 160, and 250 kDa that have been previously reported in 3T3-L1 adipocytes (36). Several of these were increased in intensity in Tfam knockdown cells in response to insulin (Fig. 8*C*, *arrowheads*), consistent with the increased phosphorylation of Akt (Fig. 6). However, one phosphoprotein, at ~49 kDa, seen at higher exposures, was significantly decreased in response to Tfam knockdown (Fig. 8*D*, *arrow*). Preliminary experiments using antibodies and siRNA to a previously identified 47-kDa Akt substrate (38) suggest that the Tfam-sensitive phosphoprotein is different and has not been previously identified. These results indicate that, whereas most signal transduction events downstream of insulin receptor activation and Akt phosphorylation are not impaired by Tfam knockdown, at least one specific protein is impaired under these conditions. This impairment correlates with the observed inhibition of insulin-stimulated glucose uptake, but more experiments, including the positive identification of this protein, will be required to establish a causal correlation between these two events.

DISCUSSION

A possible relationship between mitochondrial levels and adipose tissue function has been inferred from results in animals and humans indicating that alterations in mitochondrial levels correlate with changes in insulin sensitivity (9, 10, 15–23). In this report we have turned to a simple model, 3T3-L1 adipocytes, to determine whether a direct relationship between mitochondrial function and insulin sensitivity might indeed exist. Our results indicate that impaired induction of Tfam during differentiation results in cells with a relative deficiency in respiratory chain function but that still display many of the phenotypic characteristics of normal adipocytes. However, these cells have a reduced responsiveness to the stimulatory action of insulin on glucose transport. These results strongly suggest a specific link between respiratory chain function and glucose transport in adipose cells.

An unexpected finding in this study is that insulin stimulation of Akt phosphorylation is significantly increased in the Tfam-depleted cells. Thus, impairment of insulin action on glucose transport in cells depleted of Tfam is not due to defects in the early steps of the insulin-signaling pathway. This finding reveals a direct link between mitochondrial function and insulin action, where the activity of the respiratory chain impacts negatively upon insulin signaling to Akt. Importantly, these results are consistent with those seen in mice lacking apoptosis-inducing factor in muscle and liver, which display a progressive decrease in mitochondrial respiratory chain function (39), but have increased insulin sensitivity assessed by Akt phosphorylation and insulin tolerance. These findings as well as ours are also consistent with the finding that muscle-specific Tfam knockout mice have enhanced glucose tolerance (40), possibly resulting from improved insulin signaling. Thus, in muscle, liver, and 3T3-L1 adipocytes, a progressive defect in respiratory chain function results in enhanced insulin stimulation of Akt phosphorylation.

However, in contrast to that observed *in vivo* in muscle or liver of mice, glucose transport is clearly impaired in 3T3-L1 cells with respiratory chain deficiency. One potential cause for this difference is that the levels of GLUT4 and GLUT1 transporters are increased in muscle and liver of respiratory chain-deficient mice (39), yet no increase in expression of these transporters is seen in Tfam-depleted 3T3-L1 adipocytes. Moreover, compensatory mechanisms involving other tissues and longer adaptation times may resolve an initial impairment in insulin-

stimulated glucose transport in muscle of respiratory chain-deficient mice. It also remains possible that the response of muscle and adipose tissue to respiratory chain dysfunction may differ *in vivo*. Further work to determine the effect of adipose-tissue-specific impairment of mitochondrial function on glucose homeostasis in whole animals will be required to answer these questions. Nevertheless, the results presented here provide evidence that, in adipose cells, impaired respiratory chain function results in impaired insulin-stimulated glucose transport under conditions where compensatory adaptative mechanisms are minimized.

The results shown here point to independent links between mitochondrial function, insulin signaling, and glucose transporter trafficking. The mechanisms by which a relative deficiency in respiratory chain activity could lead to enhanced insulin signaling to Akt are not known but are areas of great interest. Mitochondrial products that are known to enhance Akt phosphorylation include H_2O_2 and perhaps other ROS (41, 42). However, we do not see any increase in ROS in Tfam KO cells (Fig. 7), and elevated ROS was not seen in tissues from apoptosis-inducing factor knockout mice (39), perhaps reflecting the requirement for integrity of the electron transport chain for ROS production (43–45). Elucidating the mechanisms that link mitochondrial respiratory chain deficiency to enhanced insulin signaling will require identification of the potential compensatory pathways elicited in by Tfam depletion in adipose cells.

With respect to the mechanisms by which Tfam knockdown might lead to impaired glucose transport despite enhanced insulin signaling to Akt, the results shown here using antibodies directed to phospho-Akt substrates suggest the possibility that mitochondrial dysfunction might affect specific substrates potentially involved in GLUT4 translocation. A clear defect in the insulin-stimulated phosphorylation of a substrate of ~49 kDa is seen in Tfam knockdown cells, which correlates with the impairment in insulin-stimulated glucose transport. Although Akt substrates such as AS160 have been shown to be important in insulin-stimulated GLUT4 translocation (46–48), additional factors are clearly necessary to mediate the full effect of insulin, and Tfam-sensitive pp 49 may be one of them. Further efforts to identify this substrate are ongoing.

In summary, two distinct functional relationships are revealed in these studies; first, a link between mitochondrial function and insulin signaling, in which impaired respiratory chain activity enhances insulin signaling to Akt phosphorylation, and second, a link between mitochondrial function and glucose transporter trafficking, where impairment of respiratory chain function leads to impaired GLUT4 translocation, perhaps through specific defects in phosphorylation of one or more Akt downstream substrates. The net result of these effects is impairment in insulin-stimulated glucose transport in adipocytes. Although further work is necessary to assess the effects of impaired adipocyte mitochondrial function on whole body glucose homeostasis, our results indicate that such impairment can be a primary cause of insulin-resistant glucose transport at a cellular level.

Acknowledgments—We thank My Chouinard for excellent technical assistance and James Young for valuable discussions.

REFERENCES

1. Unger, R. H. (2003) *Endocrinology* **144,** 5159–5165
2. Rasouli, N., Molavi, B., Elbein, S. C., and Kern, P. A. (2007) *Diabetes Obes. Metab.* **9,** 1–10
3. Ravussin, E., and Smith, S. R. (2002) *Ann. N. Y. Acad. Sci.* **967,** 363–378
4. Kim, J. Y., van de Wall, E., Laplante, M., Azzara, A., Trujillo, M. E., Hofmann, S. M., Schraw, T., Durand, J. L., Li, H., Li, G., Jelicks, L. A., Mehler, M. F., Hui, D. Y., Deshaies, Y., Shulman, G. I., Schwartz, G. J., and Scherer, P. E. (2007) *J. Clin. Invest.* **117,** 2621–2637
5. Rajala, M. W., and Scherer, P. E. (2003) *Endocrinology* **144,** 3765–3773
6. Trujillo, M. E., and Scherer, P. E. (2005) *J. Intern. Med.* **257,** 167–175
7. Picard, F., and Guarente, L. (2005) *Int. J. Obes.* (*Lond.*) **29,** Suppl. 1, S36–S39
8. Linford, N. J., Beyer, R. P., Gollahon, K., Krajcik, R. A., Malloy, V. L., Demas, V., Burmer, G. C., and Rabinovitch, P. S. (2007) *Aging Cell* **6,** 673–688
9. Wilson-Fritch, L., Burkart, A., Bell, G., Mendelson, K., Leszyk, J., Nicoloro, S., Czech, M., and Corvera, S. (2003) *Mol. Cell. Biol.* **23,** 1085–1094
10. Kaaman, M., Sparks, L. M., van Harmelen, V., Smith, S. R., Sjolin, E., Dahlman, I., and Arner, P. (2007) *Diabetologia* **50,** 2526–2533
11. Hresko, R. C., Heimberg, H., Chi, M. M., and Mueckler, M. (1998) *J. Biol. Chem.* **273,** 20658–20668
12. Reshef, L., Olswang, Y., Cassuto, H., Blum, B., Croniger, C. M., Kalhan, S. C., Tilghman, S. M., and Hanson, R. W. (2003) *J. Biol. Chem.* **278,** 30413–30416
13. Beale, E. G., Antoine, B., and Forest, C. (2003) *Trends Biochem. Sci.* **28,** 402–403
14. Choo, H. J., Kim, J. H., Kwon, O. B., Lee, C. S., Mun, J. Y., Han, S. S., Yoon, Y. S., Yoon, G., Choi, K. M., and Ko, Y. G. (2006) *Diabetologia* **49,** 784–791
15. Flachs, P., Horakova, O., Brauner, P., Rossmeisl, M., Pecina, P., Franssen-van Hal, N., Ruzickova, J., Sponarova, J., Drahota, Z., Vlcek, C., Keijer, J., Houstek, J., and Kopecky, J. (2005) *Diabetologia* **48,** 2365–2375
16. Boden, G., Homko, C., Mozzoli, M., Showe, L. C., Nichols, C., and Cheung, P. (2005) *Diabetes* **54,** 880–885
17. Bogacka, I., Xie, H., Bray, G. A., and Smith, S. R. (2005) *Diabetes* **54,** 1392–1399
18. Dahlman, I., Forsgren, M., Sjogren, A., Nordstrom, E. A., Kaaman, M., Naslund, E., Attersand, A., and Arner, P. (2006) *Diabetes* **55,** 1792–1799
19. Bogacka, I., Ukropcova, B., McNeil, M., Gimble, J. M., and Smith, S. R. (2005) *J. Clin. Endocrinol. Metab.* **90,** 6650–6656
20. Sorbris, R., Monti, M., Nilsson-Ehle, P., and Wadso, I. (1982) *Metabolism* **31,** 973–978
21. Wilson-Fritch, L., Nicoloro, S., Chouinard, M., Lazar, M. A., Chui, P. C., Leszyk, J., Straubhaar, J., Czech, M. P., and Corvera, S. (2004) *J. Clin. Invest.* **114,** 1281–1289
22. Katic, M., Kennedy, A. R., Leykin, I., Norris, A., McGettrick, A., Gesta, S., Russell, S. J., Bluher, M., Maratos-Flier, E., and Kahn, C. R. (2007) *Aging Cell* **6,** 827–839
23. Laplante, M., Festuccia, W. T., Soucy, G., Gelinas, Y., Lalonde, J., Berger, J. P., and Deshaies, Y. (2006) *Diabetes* **55,** 2771–2778
24. Falkenberg, M., Larsson, N. G., and Gustafsson, C. M. (2007) *Annu. Rev. Biochem.* **76,** 679–699
25. Asin-Cayuela, J., and Gustafsson, C. M. (2007) *Trends Biochem. Sci.* **32,** 111–117
26. Scarpulla, R. C. (2006) *J. Cell. Biochem.* **97,** 673–683
27. Kang, D., Kim, S. H., and Hamasaki, N. (2007) *Mitochondrion* **7,** 39–44
28. Larsson, N. G., Wang, J., Wilhelmsson, H., Oldfors, A., Rustin, P., Lewandoski, M., Barsh, G. S., and Clayton, D. A. (1998) *Nat. Genet.* **18,** 231–236
29. Kanehisa, M., Araki, M., Goto, S., Hattori, M., Hirakawa, M., Itoh, M., Katayama, T., Kawashima, S., Okuda, S., Tokimatsu, T., and Yamanishi, Y. (2008) *Nucleic Acids Res.* **36,** D480–D484 (database issue)
30. Axelrod, D. (2001) *Traffic* **2,** 764–774
31. Huang, S., Lifshitz, L. M., Jones, C., Bellve, K. D., Standley, C., Fonseca, S., Corvera, S., Fogarty, K. E., and Czech, M. P. (2007) *Mol. Cell. Biol.* **27,** 3456–3469
32. Bashan, N., Burdett, E., Guma, A., Sargeant, R., Tumiati, L., Liu, Z., and Klip, A. (1993) *Am. J. Physiol.* **264,** C430–C440

33. Koh, E. H., Park, J. Y., Park, H. S., Jeon, M. J., Ryu, J. W., Kim, M., Kim, S. Y., Kim, M. S., Kim, S. W., Park, I. S., Youn, J. H., and Lee, K. U. (2007) *Diabetes* **56,** 2973–2981
34. Nishikawa, T., and Araki, E. (2007) *Antioxid. Redox Signal.* **9,** 343–353
35. Imoto, K., Kukidome, D., Nishikawa, T., Matsuhisa, T., Sonoda, K., Fujisawa, K., Yano, M., Motoshima, H., Taguchi, T., Tsuruzoe, K., Matsumura, T., Ichijo, H., and Araki, E. (2006) *Diabetes* **55,** 1197–1204
36. Gridley, S., Lane, W. S., Garner, C. W., and Lienhard, G. E. (2005) *Cell. Signal.* **17,** 59–66
37. Kane, S., Sano, H., Liu, S. C., Asara, J. M., Lane, W. S., Garner, C. C., and Lienhard, G. E. (2002) *J. Biol. Chem.* **277,** 22115–22118
38. Chavez, J. A., Gridley, S., Sano, H., Lane, W. S., and Lienhard, G. E. (2006) *Biochem. Biophys. Res. Commun.* **342,** 1218–1222
39. Pospisilik, J. A., Knauf, C., Joza, N., Benit, P., Orthofer, M., Cani, P. D., Ebersberger, I., Nakashima, T., Sarao, R., Neely, G., Esterbauer, H., Kozlov, A., Kahn, C. R., Kroemer, G., Rustin, P., Burcelin, R., and Penninger, J. M. (2007) *Cell* **131,** 476–491
40. Wredenberg, A., Freyer, C., Sandstrom, M. E., Katz, A., Wibom, R., Westerblad, H., and Larsson, N. G. (2006) *Biochem. Biophys. Res. Commun.* **350,** 202–207
41. Martindale, J. L., and Holbrook, N. J. (2002) *J. Cell. Physiol.* **192,** 1–15
42. Kwon, J., Lee, S. R., Yang, K. S., Ahn, Y., Kim, Y. J., Stadtman, E. R., and Rhee, S. G. (2004) *Proc. Natl. Acad. Sci. U. S. A.* **101,** 16419–16424
43. Brunelle, J. K., Bell, E. L., Quesada, N. M., Vercauteren, K., Tiranti, V., Zeviani, M., Scarpulla, R. C., and Chandel, N. S. (2005) *Cell Metab.* **1,** 409–414
44. Guzy, R. D., Hoyos, B., Robin, E., Chen, H., Liu, L., Mansfield, K. D., Simon, M. C., Hammerling, U., and Schumacker, P. T. (2005) *Cell Metab.* **1,** 401–408
45. Mansfield, K. D., Guzy, R. D., Pan, Y., Young, R. M., Cash, T. P., Schumacker, P. T., and Simon, M. C. (2005) *Cell Metab.* **1,** 393–399
46. Karlsson, H. K., Zierath, J. R., Kane, S., Krook, A., Lienhard, G. E., and Wallberg-Henriksson, H. (2005) *Diabetes* **54,** 1692–1697
47. Zeigerer, A., McBrayer, M. K., and McGraw, T. E. (2004) *Mol. Biol. Cell* **15,** 4406–4415
48. 48 Sano, H., Kane, S., Sano, E., Miinea, C. P., Asara, J. M., Lane, W. S., Garner, C. W., and Lienhard, G. E. (2003) *J. Biol. Chem.* **278,** 14599–14602

Metabolism and Bioenergetics:

Paradoxical Effect of Mitochondrial Respiratory Chain Impairment on Insulin Signaling and Glucose Transport in Adipose Cells

Xiarong Shi, Alison Burkart, Sarah M. Nicoloro, Michael P. Czech, Juerg Straubhaar and Silvia Corvera

J. Biol. Chem. 2008, 283:30658-30667.
doi: 10.1074/jbc.M800510200 originally published online September 8, 2008